Journal of Alloys and Compounds, 194 (1993) 251–261
JALCOM 7222

Solid state amorphization of intermetallic compounds by hydrogenation*

K. Aoki and T. Masumoto
Institute for Materials Research, Tohoku University, Sendai 980 (Japan)

(Received January 21, 1992; in final form July 15, 1992)

Abstract

Recent studies on the solid state amorphization of intermetallic compounds induced by hydrogenation are described. The crystal structures and chemical compositions of the amorphizing intermetallic compounds, the formation conditions and formation processes of amorphous metallic hydrides, the mechanism of amorphization and the factors controlling the occurrence of amorphization in C15 Laves compounds are discussed.

1. Introduction

Solid state amorphization of intermetallic compounds induced by hydrogenation, *i.e.* hydrogen-induced amorphization (HIA), has recently received much attention as a novel preparation method of amorphous metallic hydrides. HIA was first demonstrated by Yeh *et al.* [1] in metastable Zr_3Rh with the $L1_2$ structure. Subsequently, we have reported that hydrogenation of C15 Laves compounds RM_2 (R ≡ a rare earth metal, M ≡ Ni, Co) gives rise to amorphization around room temperature [2, 3]. The progress of HIA in the $L1_2$-type Zr_3Al compound was observed *in situ* by high-voltage transmission electron microscopy [4]. Although it has been suggested that amorphous metallic hydrides can be formed by hydrogenation of intermetallic compounds [5, 6], experimental results on HIA have been limited to the above alloy systems with cubic (C15 and $L1_2$) structures. The experimental conditions, mechanism and process of HIA are still uncertain. In order to understand the nature of HIA, it is useful to determine the types of amorphizing intermetallic compounds and the formation conditions of amorphous metallic hydrides by hydrogenation. In this paper, the types (crystal structures, chemical compositions, formation modes and thermal stabilities (decomposition or melting temperature)) of amorphizing intermetallic compounds and the formation conditions and formation processes of amorphous alloys are described. Furthermore, the mechanism and process of HIA and the factors controlling HIA in the C15 Laves compounds are discussed.

2. Formation of amorphous metallic hydrides by hydrogenation

2.1. Structural changes of intermetallic compounds on hydrogenation

Structural changes of A_xB_{1-x} compounds (where A is a hydride-forming element such as rare earth metals, Zr, Ti, Hf, Ca and Mg and B is a non-hydride-forming element such as Al, Ga, In, Mn, Fe, Co, Ni, Cu, Ag, Sn and Pb) induced by hydrogenation were examined by X-ray diffraction (XRD), transmission electron microscopy (TEM), differential scanning calorimetry (DSC) and hydrogen analysis. The structural changes of $GdFe_2$ and Zr_3Al on hydrogenation are shown in Figs. 1 and 2 as examples.

Figure 1 shows powder XRD patterns of $GdFe_2$ with the C15 Laves ($MgCu_2$-type) structure hydrogenated at various temperatures. $GdFe_2$ absorbs hydrogen in the crystalline state at 300 K and the Bragg peaks shift to lower angles indicating the volume expansion of the lattice. In the XRD pattern of the sample hydrogenated at 423 K, however, the Bragg peaks disappear and are replaced by a broad maximum. The bright-field image of such a sample is featureless and the corresponding diffraction pattern shows a diffuse halo characteristic of amorphous alloys. Furthermore, the DSC curve shows an exothermic peak of crystallization. These observations indicate the amorphous nature of the sample. At higher hydrogenation temperatures above 673 K, new Bragg peaks corresponding to GdH_2 and α-Fe appear.

*Paper presented at the Symposium on Solid State Amorphizing Transformations, TMS Fall Meeting, Cincinnati, OH, October 21–24, 1991.

0925-8388/93/$6.00

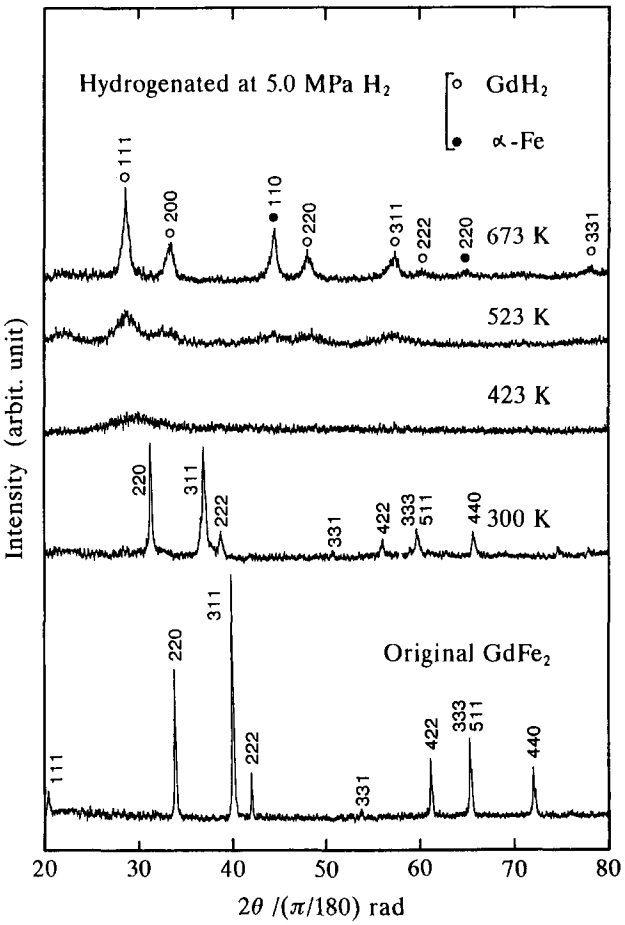

Fig. 1. Powder XRD patterns of $GdFe_2$ hydrogenated at various temperatures.

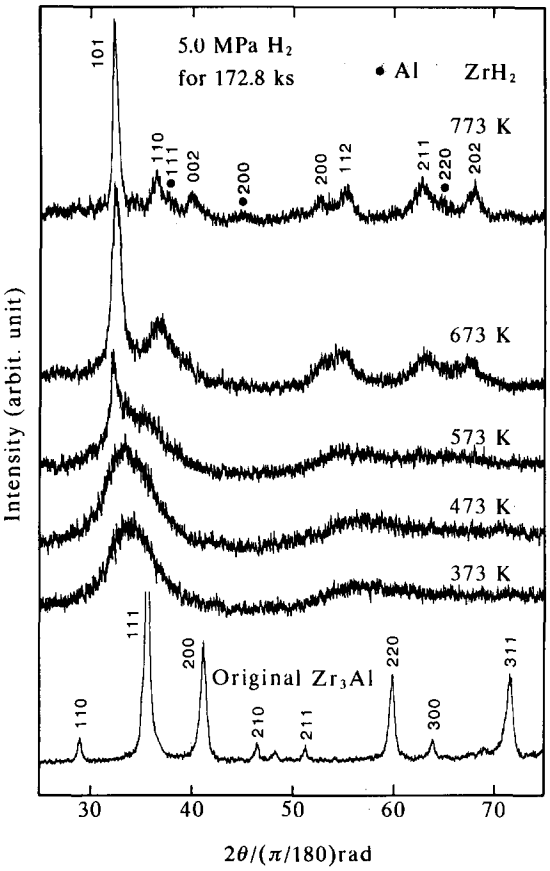

Fig. 2. Powder XRD patterns of Zr_3Al hydrogenated at various temperatures.

Figure 2 shows powder XRD patterns of Zr_3Al before and after hydrogenation [7]. Most Bragg peaks in the pattern of the original sample can be indexed to the $L1_2$ structure. The presence of all superlattice peaks indicates a high degree of long-range order in this compound. The XRD patterns of the samples hydrogenated at 373 and 473 K do not show Bragg peaks but a broad maximum. TEM of such samples supports their amorphous nature. At higher temperatures, Zr_3Al decomposes into pure Al and ZrH_2.

Figure 3 shows XRD patterns of Zr_3Al hydrogenated at 473 K for 43.2 and 172.8 ks. The appearance of the small, broad diffraction maximum close to the (111) fundamental peak in the sample hydrogenated for 43.2 ks indicates that the hydrogenated alloy has been partially amorphized. The disappearance of the superlattice peaks suggests that chemical disordering plays an important role in HIA as in irradiation-induced amorphization [8], although it has recently been reported that the dominant effect of hydrogen absorption in Zr_3Al is a substantial lattice expansion with no appreciable loss in the long-range order [9].

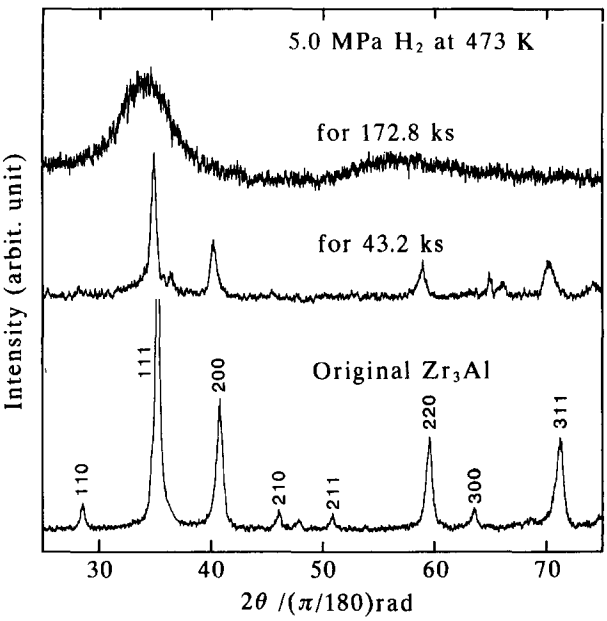

Fig. 3. Powder XRD patterns of Zr_3Al hydrogenated for 43.2 ks and 172.8 ks at 473 K.

2.2. Chemical compositions and crystal structures of amorphizing intermetallic compounds

The phases of the A_xB_{1-x} compounds formed on hydrogenation at 300, 400 and 600 K are given, together

with the chemical compositions and crystal structures of the original compounds in Table 1 [10–12]. The formation modes and thermal stabilities (the decomposition temperatures or the melting points) of the typical compounds are also listed. As seen in Table 1, more than 60 compounds can amorphize by hydrogenation at room temperature. Amorphizing compounds have the A_3B-, A_2B- and AB_2-type compositions, but no amorphization is observed in the AB-, AB_3- and AB_5-type compounds.

In the A_3B-type compounds, $L1_2$ compounds, such as Zr_3M (M ≡ In, Al, Rh) and R_3In (R ≡ rare earth metal), and $D0_{19}$ compounds, such as R_3Ga and R_3Al, amorphize. The $D0_{19}$ compounds R_3Ga transform to the $L1_2$-type c-R_3GaH_x and the $L1_2$ compound Zr_3In changes to f.c.c. c-Zr_3InH_x at elevated temperatures ("c" indicates crystalline).

In the A_2B-type compounds, C23 compounds such as R_2Al and $B8_2$ compounds such as R_2In and Zr_2Al amorphize.

In the AB_2-type compounds, only C15 Laves compounds amorphize. Among the C15 Laves compounds, RM_2 compounds (M ≡ Fe, Co, Ni) amorphize, but RAl_2, ZrV_2 and others do not. Thus HIA is confined to intermetallic compounds with specific crystal structures in contrast with other solid state amorphization reactions (SSARs). These experimental results suggest that HIA occurs when hydrogen atoms are in special environments, which may be directly related to the mechanism of HIA.

2.3. Factors controlling the occurrence of HIA in the C15 Laves compounds

Not all compounds having the specific crystal structures, *e.g.* C15, C23, $L1_2$, $B8_2$ and $D0_{19}$, are amorphized by hydrogenation. For example, the C15 Laves compounds RM_2 (R ≡ a rare earth metal, M ≡ Fe, Co, Ni) amorphize on hydrogenation around 400–500 K [2–7, 10–13], but ZrV_2, $ZrMo_2$ and others absorb hydrogen and retain the crystalline state as mentioned previously. Consequently, HIA is considered to be controlled not only by the crystal structure, but also by other factors. In the present work, the factors controlling the formation of the amorphous metallic hydrides were analysed. Several factors, such as the atomic size ratio, electron concentration, thermal stability of the original compounds and size of the tetrahedral holes occupied by the hydrogen atoms were examined.

The states of the hydrogenated C15 Laves compounds are plotted in the interstitial hole size *vs.* thermal stability (decomposition temperature or melting point of the original compounds) diagram (Fig. 4). Here, the radii $r_{h(G)}$ of interstitial holes were calculated using the Goldschmidt radii for the tetrahedral A_2B_2 holes. The filled and open circles show the amorphous and crystalline states respectively. As can be seen in Fig. 4, the compounds having a hole size $r_{h(G)}$ above 0.0335 nm and a decomposition temperature below about 1650 K are amorphized by hydrogenation. According to Westlake [14] the metals absorb hydrogen into the holes when $0.033\ \text{nm} < r_h < 0.043\ \text{nm}$. The present minimum hole size, 0.0335 nm, for HIA in the C15 Laves compounds is in good agreement with Westlake's empirical minimum hole size for hydrogen absorption. Therefore HIA is not considered to occur in compounds with hole sizes below 0.033 nm because hydrogen is not absorbed.

In order for HIA to occur, the metal–metal bond in the compounds must be broken. If the bond is too strong, HIA may not occur. As a measure of the strength of the bond, we employed the decomposition (or melting) temperatures of the original compounds. The reason why the thermally stable compounds, *i.e.* with decomposition temperatures above 1650 K, are not amorphized can be explained by the difficulty in breaking of the metal–metal bond. Thus the formation of amorphous metallic hydrides in the C15 compounds can be expressed by a combination of the hole size calculated using the Goldschmidt radii and the thermal stability of the original compounds.

The AB_2 Laves phases are so-called size factor compounds and are constructed from the close packing of hard spheres with the ideal atomic size ratio R_A/R_B of 1.225. In reality, the ratio is known to vary between 1.05 and 1.68. Substantial mutual adjustments of the atomic size can take place when the compounds are formed by atomic species whose radius ratio does not coincide with the ideal value. The parameters $(r_A - R_A)$ and $(r_B - R_B)$ have been employed as indices of the size adjustments. Here, r_A and r_B are the radii of the A and B atoms calculated from the lattice parameters and the packing geometry of the C15 Laves compounds, *i.e.* $r_A = (3)^{1/2}a/8$ and $r_B = (2)^{1/2}a/8$, and R_A and R_B are the Goldschmidt radii of the A and B atoms. When R_A/R_B is greater than the ideal ratio 1.225, the A atoms exhibit a size contraction ($(r_A - R_A) < 0$) and are under compression, and when the ratio is less than the ideal the A atoms show an increase in their effective size ($(r_A - R_A) > 0$) and are under tension. The B atoms show a reverse trend, expanding in size when R_A/R_B is greater than the ideal value and contracting when the ratio is less than the ideal value.

The states of the hydrogenated C15 Laves compounds are plotted as a function of the parameters $(r_A - R_A)$, $(r_B - R_B)$ and R_A/R_B in Figs. 5 and 6. As can be seen the compounds with an atomic size ratio above 1.37 are amorphized by hydrogenation without exception.

The values of $(r_A - R_A)$ decrease with increasing R_A/R_B values, i.e. the A atoms contract as the atomic size ratio becomes large as shown in Fig. 5. HIA occurs

TABLE 1. Chemical compositions, crystal structures and states of intermetallic compounds hydrogenated at 300, 400 and 600 K and formation modes and melting (or decomposition) temperatures of typical compounds

Composition	Structure	Compounds	Formation mode of compounds (decomposition temp.)	Formation phases		
				300 K	400 K	600 K
A_3B	$L1_2$	Zr_3In	Peritectoid (1248 K)			Zr_3InH_x (f.c.c.)
	or	Zr_3Al			Am	
	f.c.c.	Zr_3Rh	Metastable (rapid quenching)	Am	Am	$RH_2 + RIn_3$ ($L1_2$)
		R_3In (R ≡ Ce, Pr, Nd, Sm)	Peritectoid (Pr_2In, 1040 K)			$RH_2 + RIn_3$ ($L1_2$)
	$D0_{19}$	R_3Ga (R ≡ La, Pr, Nd, Sm)	Peritectic (Nd_3Ga, 1059 K)	Am	Am	R_3GaH_x ($L1_2$)
		R_3Al (R ≡ La, Ce, Ce, Pr, Nd)	Peritectic (Nd_3Al, 948 K)	Am	Am	$RH_2 + RAl_2$ (C15)
A_2B	C23	R_2Al (R ≡ Y, Pr, Nd, Sm, Gd, Tb, Dy, Ho)	Peritectic (Ga_2Al, 1223 K)	Am	Am	$RH_2 + RAl_2$ (C15)
	$B8_2$	R_2In (R ≡ La, Ce, Nd, Sm, Gd, Tb, Dy, Ho, Er)	Congruent (Gd_2In, 1463 K)	Am	Am	$RH_2 + RIn_3$ ($L1_2$)
		Zr_2Al	Peritectoid (1523 K)	Am		
AB_2	C15	RFe_2 (R ≡ Y, Sm, Gd, Tb, Dy, Ho, Er)	Peritectic ($GdFe_2$, 1353 K)	c-RFe_2H_x	Am	$RH_2 + \alpha$-Fe
		$CeFe_2$	Peritectic (1046 K)	Am	Am	$CeH_2 + \alpha$-Fe
		RCo_2 (R ≡ Y, Ce, Pr, Nd, Sm, Gd, Tb, Dy, Ho, Er)	Peritectic ($GdCo_2$, 1373 K)	c-RCo_2H_x	Am	$RH_2 + Co$
		RNi_2 (R ≡ Y, Ce, Pr, Nd, Sm, Gd, Tb, Dy, Ho, Er)		Am	Am	$RH_2 + RNi_5$
		$LaNi_2$	Metastable phase	Am	Am	$LaH_2 + LaNi_5$
		RMn_2 (R ≡ Y, Gd, Dy, Ho)	Peritectic ($GdMn_2$, 1223 K)	c-RMn_2H_x	Am	$RH_2 + Mn$

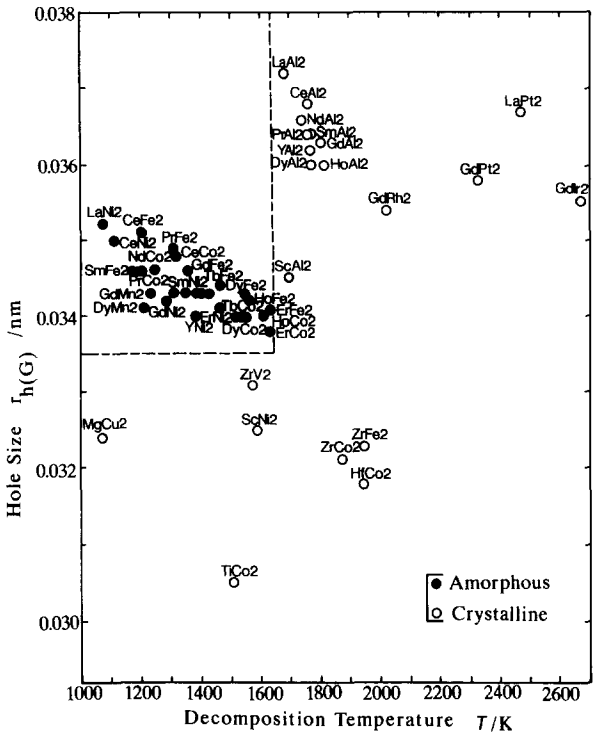

Fig. 4. States of the hydrogenated C15 Laves compounds as a function of the radius $r_{h(G)}$ of the tetrahedral holes and the thermal stability (decomposition temperature or melting point) of the original compounds.

when the A atoms undergo strong size contraction. In contrast, the values of $(r_B - R_B)$ increase with increasing R_A/R_B values as shown in Fig. 6. The B atoms exhibit size contraction ($(r_B - R_B) < 0$) when R_A/R_B is smaller than 1.37, but show an increase in effective size ($(r_B - R_B) > 0$) when R_A/R_B is larger than 1.37. HIA occurs under such conditions. Thus both the large contraction of the A atoms and the expansion of the B atoms are closely related to the occurrence of HIA.

As shown in Fig. 4, the formation range of hydrogen-induced amorphous hydrides can be expressed by a combination of hole size and thermal stability (decomposition temperatures) of the original compounds. However, the occurrence of HIA is not expressed solely by either the hole size or the thermal stability of the compounds. Consequently, it is concluded that the atomic size ratio is the single most important factor controlling the occurrence of HIA in the C15 Laves AB_2 compounds, and the compounds with a ratio above 1.37 are amorphized by hydrogenation. The well-known empirical rule for the size effect states that the atomic radii of two elements must differ by more than 10% in order for their binary alloys to form amorphous alloys by rapid quenching [15]. The difference (37%) in the atomic sizes required for the occurrence of HIA is much larger than that required for the formation of the amorphous alloys by rapid quenching.

2.4. Formation of amorphous metallic hydrides as a function of the hydrogen pressure and the hydrogenation temperature

The reaction products of the C15 Laves RNi_2 compounds formed on hydrogenation at various hydrogen pressures and hydrogenation temperatures for 86.4 ks, are displayed in Figs. 7–9 [13]. As can be seen in Fig. 7, a single phase of a-$SmNi_2H_x$ ("a" indicates amorphous) is formed independent of the H_2 pressure in the low-temperature region I. The compounds c-$SmNi_5$ and c-SmH_2 are formed in the high-temperature region IV. Thus the reaction products of $SmNi_2$ depend on the hydrogenation temperature not the H_2 pressure.

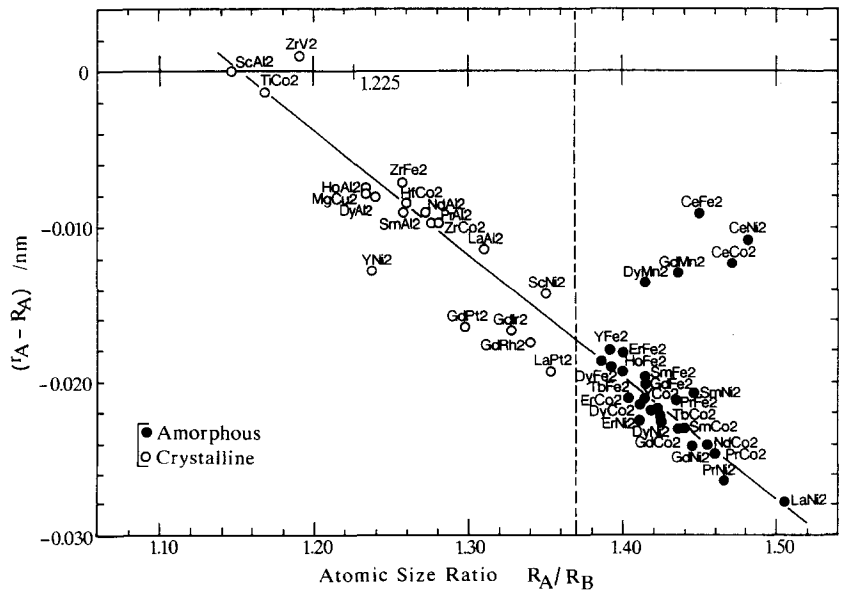

Fig. 5. States of the hydrogenated C15 Laves compounds as a function of $(r_A - R_A)$ and R_A/R_B.

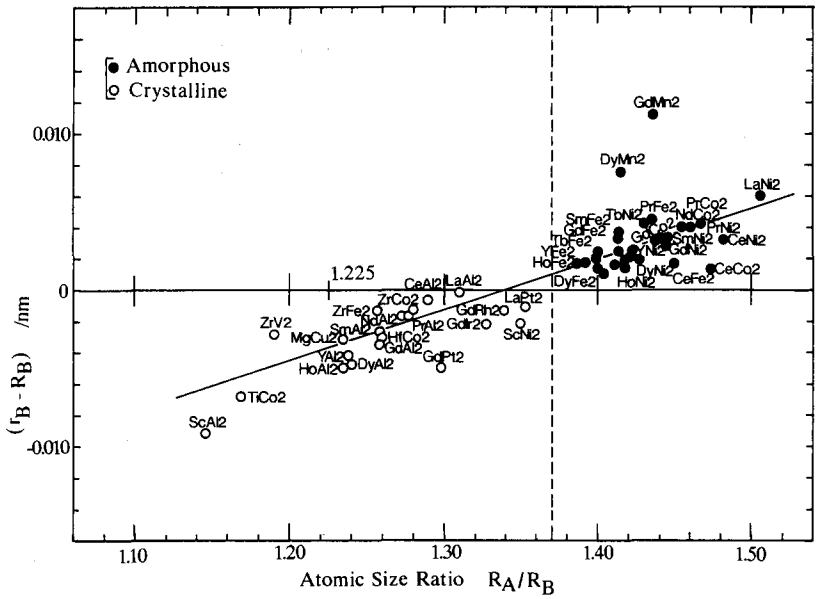

Fig. 6. States of the hydrogenated C15 Laves compounds as a function of $(r_B - R_B)$ and R_A/R_B.

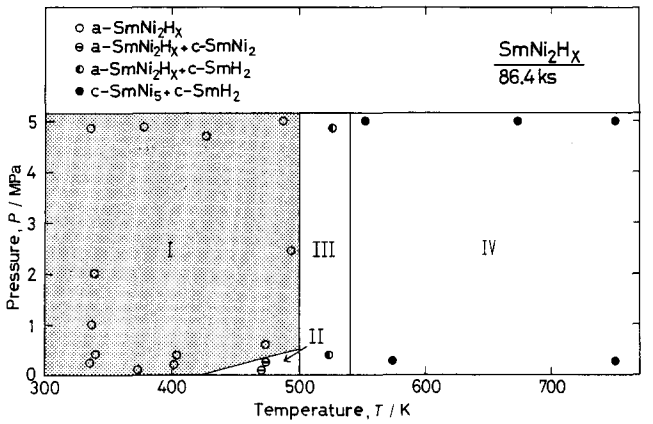

Fig. 7. Formation ranges of the reaction products on hydrogenation of $SmNi_2$ for 86.4 ks.

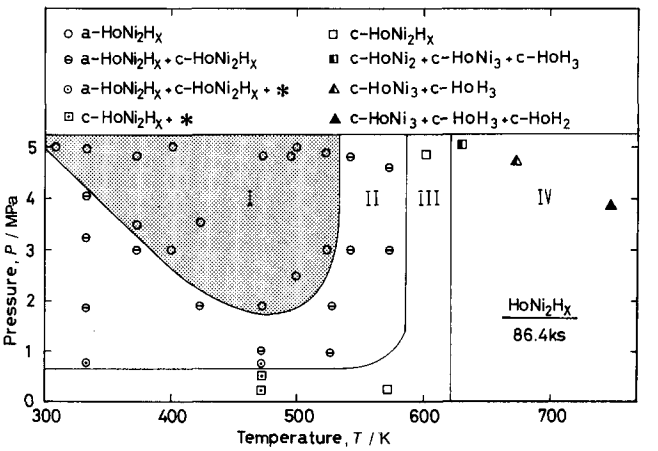

Fig. 8. Formation ranges of the reaction products on hydrogenation of $HoNi_2$ for 86.4 ks.

The reaction products of $HoNi_2$ with hydrogen gas depend on the H_2 pressure and hydrogenation temperature. A single phase of a-$HoNi_2H_x$ is formed in the high hydrogen pressure region I ($T < 523$ K, $P = 2.0$–5.0 MPa) as shown in Fig. 8. Higher gas pressures are required to form a single phase of a-$HoNi_2H_x$ at lower temperatures. A single phase of c-$HoNi_2H_x$ is formed in region III which is located at lower H_2 pressure and higher temperature. $HoNi_2$ decomposes into the compounds c-$HoNi_3$ and c-$HoNi_2$ and the hydrides c-HoH_3 and c-HoH_2 in region IV ($T > 630$ K).

The situation for $ErNi_2$ is similar to $HoNi_2$, although single-phase a-$ErNi_2H_x$ is confined to the higher hydrogen pressure region I as shown in Fig. 9. A single phase of c-$ErNi_2H_x$ is formed in region III. Thus the formation ranges of the amorphous metallic hydrides depend strongly on the hydrogen pressure, hydrogenation temperature and the type of rare earth metal.

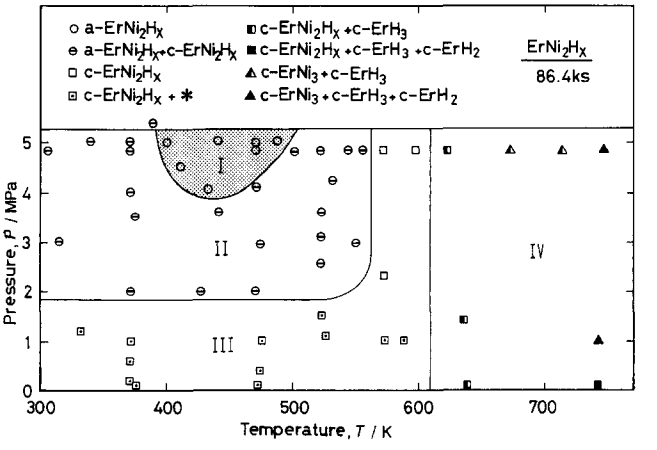

Fig. 9. Formation ranges of the reaction products on hydrogenation of $ErNi_2$ for 86.4 ks.

From these experimental results, it can be concluded that the search for new amorphizing compounds must be performed at higher hydrogen pressures.

3. Thermal analysis of HIA

3.1. Differential thermal analysis (DTA) curves of $GdFe_2$ heated in a hydrogen atmosphere

In order for the HIA reaction to proceed, an amorphous product must have a lower free energy than the corresponding crystalline product and a kinetic barrier must exist to prevent the formation of the equilibrium phase. However, the mechanism and kinetics of HIA are still uncertain. We thermally analysed $GdFe_2$ in a hydrogen atmosphere to obtain information on the thermodynamic and kinetic aspects of HIA.

Figure 10 shows the DTA curves of $GdFe_2$ heated in a hydrogen atmosphere (0.1–5.0 MPa) [16]. Four exothermic peaks are clearly observed in every curve. In contrast, no peak is detected for the samples heated in an argon atmosphere. These observations indicate that the peaks are caused by structural changes induced by the absorption or desorption of hydrogen. In order to determine the origin of the peaks, XRD, TEM, DSC and hydrogen analysis were carried out for the samples heated to the distinct stages marked by the arrows.

The DTA curve and the change in the hydrogen content for the samples heated in 1.0 MPa of hydrogen are shown in Fig. 11. By heating the sample above the

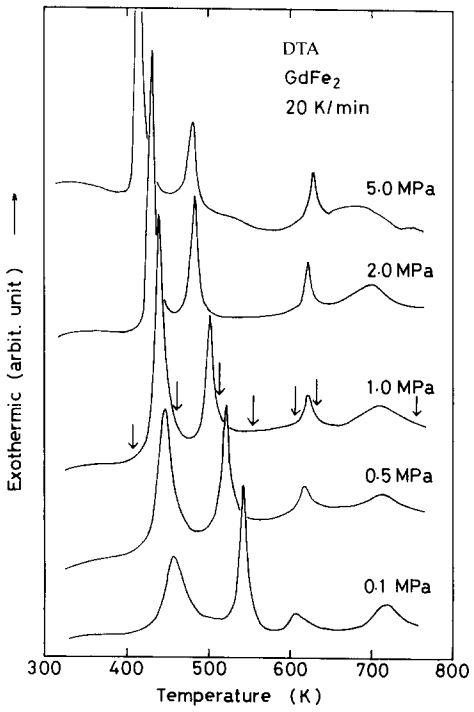

Fig. 10. DTA curves of $GdFe_2$ heated in a hydrogen atmosphere at a pressure of 0.1–5.0 MPa.

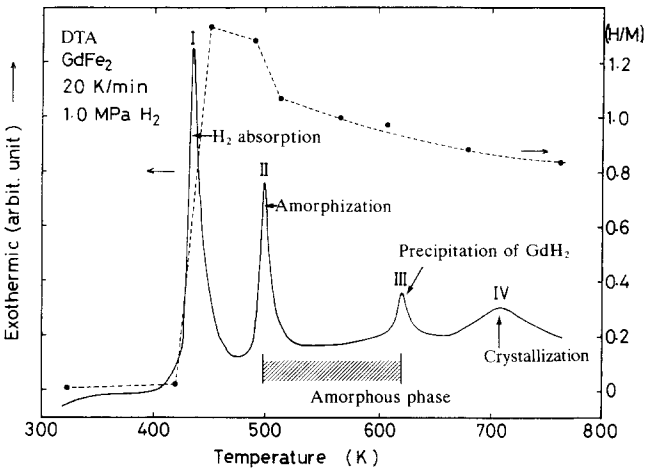

Fig. 11. DTA curve and hydrogen content in the $GdFe_2$ samples heated in 1.0 MPa hydrogen to the distinct stages shown by the arrows.

first exothermic peak (to 458 K), the hydrogen content increases rapidly from 0 to 1.37 atoms per metal atom (H/M), and the Bragg peaks shift to lower angles. From these observations, the first exothermic peak is concluded to be due to hydrogen absorption in the crystalline state, *i.e.* c-$GdFe_2$ changes to c-$GdFe_2H_4$. In the XRD patterns of the samples heated to 513–605 K, the Bragg peaks disappear and are replaced by a broad maximum. TEM confirms the amorphous nature of the samples. Furthermore, the DSC curves of these samples show exothermic peaks of crystallization. Correspondingly, the hydrogen content decreases to 1.0 (H/M). These observations indicate that the second exothermic peak is due to the transformation from c-$GdFe_2H_4$ to a-$GdFe_2H_3$, *i.e.* HIA. Since HIA occurs exothermally, we can conclude that the enthalpy of a-$GdFe_2H_3$ is lower than that of c-$GdFe_2H_4$. The sharpness of the peak implies that HIA is completed in a shorter time than other SSARs.

The TEM observations indicate that the third and fourth exothermic peaks are due to precipitation of GdH_2 in the amorphous phase and crystallization of the remaining amorphous phase respectively. The origin of each peak and the formation range of the amorphous phase are also indicated in Fig. 11. Amorphous, single-phase a-$GdFe_2H_x$ is obtained between 500 and 620 K at 1.0 MPa H_2.

3.2. Activation energy of HIA and its pressure dependence

Figure 12 shows the pressure dependence of the activation energies, determined by the Kissinger method, for hydrogen absorption, HIA and precipitation of GdH_2. As the hydrogen pressure increases from 0.1 to 5.0 MPa, E_h for hydrogen absorption and E_a for amorphization decrease from 125 to 110 kJ mol^{-1} and from 130 to 95 kJ mol^{-1} respectively. In contrast, E_p for

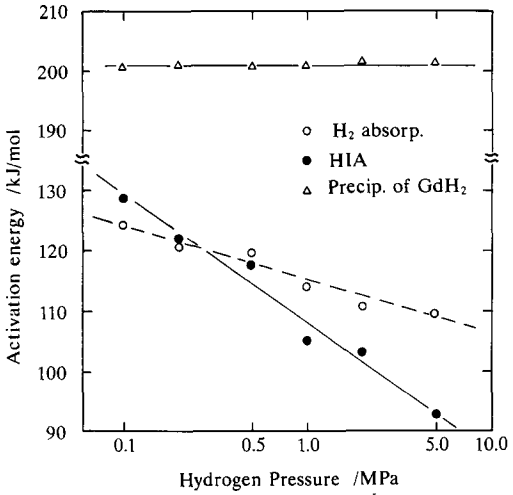

Fig. 12. Pressure dependence of the activation energy E for hydrogen absorption, amorphization and precipitation of GdH_2.

precipitation of GdH_2 is almost constant at 200 kJ mol^{-1}. The pressure dependence of the activation energies indicates that the higher the hydrogen pressure becomes, the more easily hydrogen absorption and HIA occur. It is worth noting that E_a is comparable with E_h and about one-half of the E_p value; HIA and the precipitation of GdH_2 are controlled by the movement of metal atoms, but hydrogen absorption does not require the movement of metal atoms.

We now discuss the thermodynamic driving force and the activation energy E_a for HIA. In the C15 Laves compounds c-$GdFe_2H_x$, the occupation sites of hydrogen atoms are confined geometrically to the tetrahedral sites surrounded by 2Gd+2Fe and 1Gd+3Fe [17]. In contrast, in a-$GdFe_2H_x$, hydrogen atoms can occupy the tetrahedral sites surrounded by 4Gd, 3Gd+1Fe, 2Gd+2Fe and 1Gd+3Fe [18]. Since Gd has a large negative heat of mixing with hydrogen, hydrogen atoms in the sites surrounded by 4Gd and 3Gd+1Fe, *i.e.* in the amorphous phase, are much more strongly bound. Since hydrogen atoms in the crystalline phase are less energetically favourable, rearrangements of the metallic atoms occur to reduce the total free energy of the alloys when c-$GdFe_2H_x$ is heated to a temperature where the metallic atoms can move over a short distance, *i.e.* HIA. The lowering of the activation energy E_a from 130 to 95 kJ mol^{-1} with increasing H_2 pressure indicates that the movement of the metal atoms during the transformation from c-$GdFe_2H_x$ to a-$GdFe_2H_x$ is enhanced by hydrogen. This reasoning indicates that the thermodynamic driving force for HIA in $GdFe_2$ is the enthalpy difference resulting from the different hydrogen occupation sites in the two states of the alloys. At higher temperatures, where the metallic atoms can move much more easily, the amorphous phase is no longer stable; GdH_2 precipitates or the amorphous phase decomposes into more stable phases. The precipitation of GdH_2 requires the long-range diffusion of Gd atoms. E_p may correspond to the activation energy for the diffusion of Gd atoms in a-$GdFe_2H_x$.

4. Formation process of amorphous metallic hydrides by hydrogenation

In order to clarify the formation process of the amorphous metallic hydrides, structural changes of the C15 Laves phases RNi_2 have been followed by XRD and DSC [13].

Figures 13 and 14 show the XRD patterns and DSC curves of $DyNi_2$ hydrogenated at 400 K and 5.0 MPa of hydrogen. The intensity of the Bragg peaks decreases gradually with hydrogenation time and the amorphous halo appears and grows. Since the position and width of the diffraction peaks are almost constant, we can conclude that little hydrogen is absorbed into c-$DyNi_2$ and that c-$DyNi_2H_x$ is absent. The sample becomes a-$DyNi_2H_x$ after 38.4 ks of hydrogenation.

The DSC curve of $DyNi_2$ hydrogenated for 19.5 ks shows a broad endothermic peak of hydrogen desorption (below the broken line) and an exothermic peak of crystallization. These results indicate that an amorphous phase has been formed locally by hydrogenation for 19.5 ks. Both the endothermic and exothermic peaks increase with increasing hydrogenation time. The DSC curves support the absence of c-$DyNi_2H_x$, because only a broad endothermic peak is seen in the DSC curves. We call this process non-solid-solution-type amorphi-

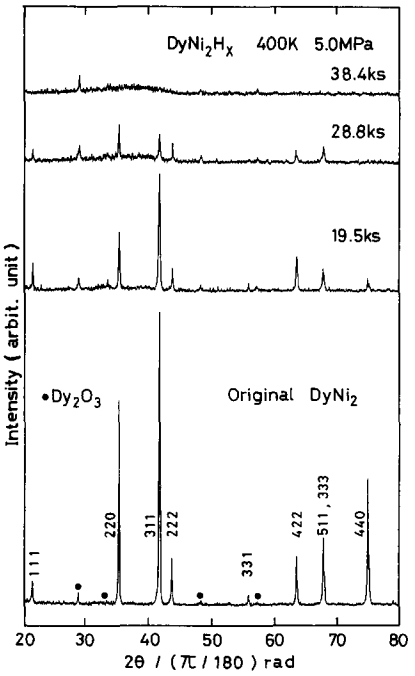

Fig. 13. XRD patterns of $DyNi_2$ hydrogenated at 400 K and 5.0 MPa of hydrogen.

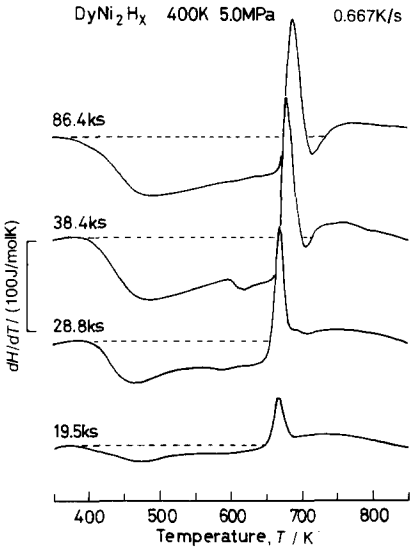

Fig. 14. DSC curves of $DyNi_2$ hydrogenated at 400 K and 5.0 MPa of hydrogen.

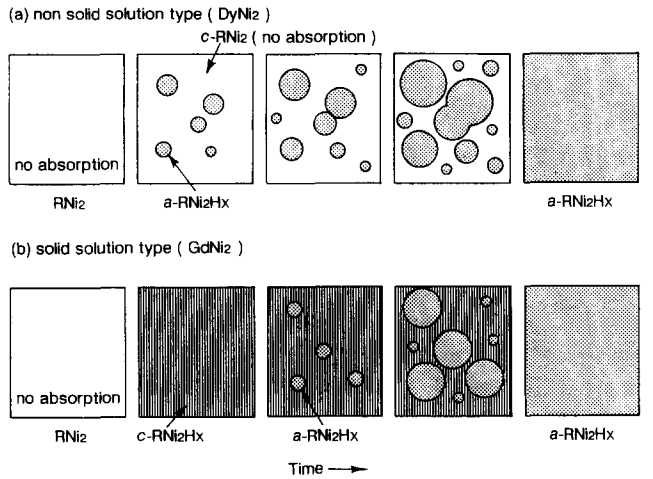

Fig. 15. Schematic diagrams of the formation process of hydrogen-induced amorphous metallic hydrides for (a) $DyNi_2$ and (b) $GdNi_2$.

zation, because hydrogen is not absorbed in the crystalline sample. $CeFe_2$ is known to amorphize by this process [19]. The process of HIA by the non-solid-solution-type process is shown schematically in Fig. 15(a). a-RNi_2H_x nucleates in the Laves phase c-RNi_2 initially and this amorphous phase increases with increasing hydrogenation time. Finally, the whole sample becomes amorphous.

The XRD patterns and DSC curves of $GdNi_2$ hydrogenated at 400 K and 2.0 MPa H_2 are shown in Figs. 16 and 17. The Bragg peaks shift to low angles on hydrogenation for 0.3 ks. The positions of the Bragg peaks are almost constant after 0.3 ks of hydrogenation but the intensity of the Bragg peaks gradually decreases with hydrogenation time. The sample changes to a-$GdNi_2H_x$ after 21.0 ks of hydrogenation.

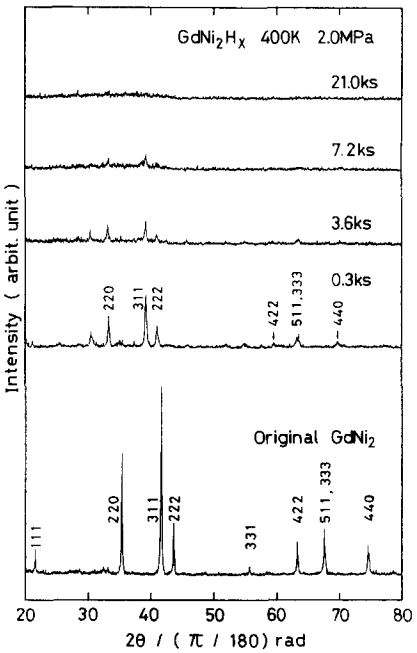

Fig. 16. XRD patterns of $GdNi_2$ hydrogenated at 400 K and 2.0 MPa of hydrogen.

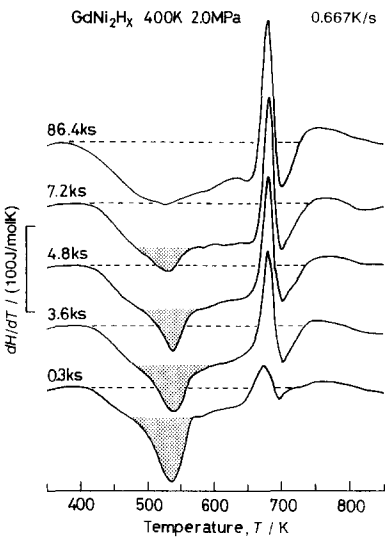

Fig. 17. DSC curves of $GdNi_2$ hydrogenated at 400 K and 2.0 MPa of hydrogen.

The DSC curve of $GdNi_2$ hydrogenated for 0.3 ks clearly shows an endothermic peak of hydrogen desorption (below the broken line) and an exothermic peak of crystallization. The broad endothermic peak below the broken line corresponds to hydrogen desorption from a-$GdNi_2H_x$, and the sharp endothermic peak indicated by the shaded area corresponds to hydrogen desorption from c-$GdNi_2H_x$. The presence of sharp and broad endothermic peaks indicates that c-$GdNi_2H_x$ coexists with a-$GdNi_2H_x$. The sharp endothermic peak disappears after 86.4 ks. These changes in XRD and DSC indicate that amorphization proceeds

by the coexistence of c-$GdNi_2H_x$ and a-$GdNi_2H_x$ as shown schematically in Fig. 15(b). The Laves phase c-RNi_2 absorbs hydrogen and changes to c-RNi_2H_x initially. Subsequently, a-RNi_2H_x nucleates in c-RNi_2H_x and increases with increasing hydrogenation time. We call this process solid-solution-type amorphization, because hydrogen is absorbed in the crystalline phase. $GdFe_2$ is amorphized by this process [16]. Thus there are two kinds of formation process of the amorphous metallic hydrides in RNi_2 Laves compounds. These two HIA processes can be analysed using the Johnson–Mehl–Avrami equation assuming that the quantity of the amorphous phase formed is proportional to the enthalpy change of crystallization.

Figure 18 shows a plot of the hydrogenation time t *vs.* the rate of transformation X. $X=\Delta H_{xt}/\Delta H_{xm}$ where ΔH_{xt} is the enthalpy change of the sample hydrogenated for ts and ΔH_{xm} is the enthalpy change for $t=86.4$ ks. We assumed that $X=1$ at $t=86.4$ ks. The data give linear plots and the numerical exponent and the rate constant are obtained as $n=3.9$, $k=3.6\times10^{-5}$ s^{-1} for $DyNi_2$ and $n=0.5$, $k=3.7\times10^{-4}$ s^{-1} for $GdNi_2$. The numerical exponent n is considered to depend on the rate-determining factor of the amorphization process. We can discuss the HIA process in terms of the n value.

(1) Non-solid-solution-type amorphization. Two kinds of rate-determining factors are assumed in HIA, *i.e.* the redistribution of metallic atoms at the interface boundaries between c-RNi_2 and a-RNi_2H_x (the interface control) and the long-range diffusion of hydrogen to the interface boundaries (the diffusion control). Since the diffusion of hydrogen atoms in metals is higher than that of metals by ten orders of magnitude, the rate-determining factor of HIA may be the redistribution of metallic atoms at the crystal–amorphous interface boundaries. The value of $n=3.9$ is similar to that for interface-controlled growth at a constant nucleation rate which takes $n=4$ [20].

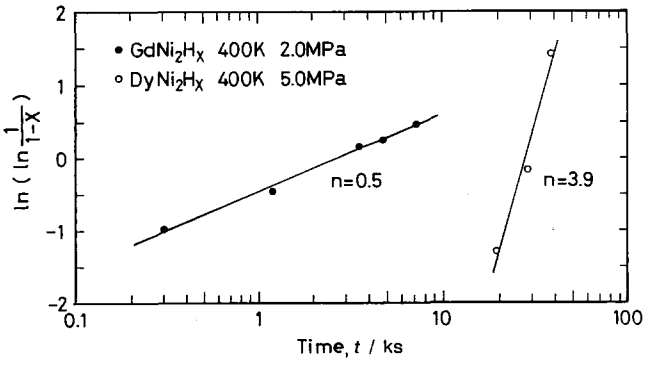

Fig. 18. Johnson–Mehl–Avrami plot for the progress of hydrogen-induced amorphization in $DyNi_2$ and $GdNi_2$.

(2) Solid-solution-type amorphization. Since the alloy composition does not change on transformation from c-RNi_2H_x to a-RNi_2H_x, this is regarded as polymorphous transformation. The polymorphous transformation is usually interface controlled and takes $n>1$. However, the value of the numerical exponent n for $GdNi_2H_x$ is 0.5. This result is not explained by interface-controlled transformation. It is suggested that solid-state-type amorphization is different from the usual nucleation–growth-type transformation.

5. Summary and conclusions

Structural changes of A_xB_{1-x} compounds (where A is a rare earth metal, Zr, Ti, Hf, Ca or Mg and B is Al, Ga, In, Mn, Fe, Co, Ni, Cu, Ag, Sn or Pb) induced by hydrogenation were examined by XRD, TEM, DSC and hydrogen analysis. Compounds amorphized by hydrogenation include the $L1_2$, $D0_{19}$, C23, $B8_2$ and C15 Laves compounds with the AB_2-, A_2B- and A_3B-type compositions. The atomic size ratio is the single most important factor controlling the occurrence of HIA in the C15 Laves AB_2 compounds and the compounds with a ratio above 1.37 are amorphized by hydrogenation. The ranges of formation of the amorphous metallic hydrides in C15 Laves RNi_2 depend strongly on the hydrogen pressure, hydrogenation temperature and the type of rare earth metal. The DTA curves of $GdFe_2$ in a hydrogen atmosphere show four exothermic peaks due to hydrogen absorption, HIA, precipitation of $GdFe_2$ and crystallization of the remaining amorphous alloys. As the hydrogen pressure increases from 0.1 to 5.0 MPa H_2, the activation energy E_a for amorphization decreases from 130 to 95 kJ mol^{-1}. The thermodynamic driving force for HIA in the C15 Laves compounds is considered to be the enthalpy difference resulting from the different hydrogen occupation sites in the two states of the alloys. There are two kinds of formation process of the amorphous metallic hydrides in RNi_2 Laves compounds, *i.e.* solid-solution-type and non-solid-solution-type amorphization. The rate-determining factors of these amorphization processes were discussed on the basis of the results obtained by the Johnson–Mehl–Avrami equation.

References

1 X. L. Yeh, K. Samwer and W. L. Johnson, *Appl. Phys. Lett.*, *42* (1983) 242.
2 K. Aoki, K. Shirakawa and T. Masumoto, *Sci. Rep. Res. Inst. Tohoku Univ. Ser. A, 32* (1985) 239.
3 K. Aoki, T. Yamamoto and T. Masumoto, *Sci. Rep. Res. Inst. Tohoku Univ. Ser. A, 33* (1986) 163.

4 H. Fujita, in H. Fujita (ed.), *Proc. Int. Symp. on Behavior of Lattice Imperfections in Metals — In situ Experimentation with HVEM, Osaka University, Japan, November 18, 1985*, p. 1.
5 H. Oesterreicher, J. Clinton and H. Bittner, *Mater. Res. Bull., 11* (1976) 1241.
6 I. Jacob and D. Shaltiel, *J. Less-Common Met., 65* (1979) 117.
7 X. G. Li, K. Aoki and T. Masumoto, *Sci. Rep. Res. Inst. Tohoku Univ. Ser. A, 35* (1990) 84.
8 P. R. Okamoto, L. E. Rehn, J. Pearson, R. Bhadra and G. Grimsdicht, *J. Less-Common Met., 140* (1988) 231.
9 W. J. Meng, P. R. Okamoto, L. J. Thompson, B. J. Kestel and L. E. Rehn, *Appl. Phys. Lett., 53* (1988) 1820.
10 K. Aoki, T. Yamamoto and T. Masumoto, *Scr. Metall., 21* (1987) 27.
11 K. Aoki, A. Yanagitani, X.-G. Li and T. Masumoto, *Mater. Sci. Eng., 97* (1988) 35.
12 K. Aoki, X.-G. Li, T. Aihara and T. Masumoto, *Mater. Sci. Eng. A, 133* (1991) 316.
13 T. Aihara, K. Aoki and T. Masumoto, *J. Jpn. Inst. Met., 54* (1990) 970.
14 D. G. Westlake, *J. Less-Common Met., 90* (1983) 251.
15 B. C. Giessen, in T. Masumoto and K. Suzuki (eds.), *Proc. 4th Int. Conf. on Rapidly Quenched Metals*, Vol. 1, Japan Institute of Metals, Sendai, 1982, p. 213.
16 K. Aoki, X.-G. Li and T. Masumoto, *Acta Metall. Mater., 40* (1992) 221.
17 D. Ivey and D. Northwood, *J. Less-Common Met., 115* (1986) 23.
18 M. Matsuura, K. Fukamichi, H. Komatsu, K. Aoki, T. Masumoto and K. Suzuki, *Mater. Sci. Eng., 97* (1988) 251.
19 K. Aoki, T. Yamamoto, Y. Sato, K. Fukamichi and T. Masumoto, *Acta Metall., 35* (1987) 2465.
20 J. W. Christian, *The Theory of Transformation in Metals and Alloys*, Pergamon, Oxford, 2nd edn., 1975, p. 542.